REPORT DOCUMENTATION PAGE

Form Approved
OMB No. 0704-0188

1. REPORT DATE *(DD-MM-YYYY)*	**2. REPORT TYPE**	**3. DATES COVERED** *(From - To)*
July 2015	Technical Paper	July 2015-July 2015

4. TITLE AND SUBTITLE
Pseudospectral model for hybrid PIC Hall-effect thruster simulationect thruster simulation

5a. CONTRACT NUMBER
In-House

5b. GRANT NUMBER

5c. PROGRAM ELEMENT NUMBER

6. AUTHOR(S)
Justin Koo, David Bilyeu and Robert Martin

5d. PROJECT NUMBER

5e. TASK NUMBER

5f. WORK UNIT NUMBER
Q0A5

7. PERFORMING ORGANIZATION NAME(S) AND ADDRESS(ES)

Air Force Research Laboratory (AFMC)
AFRL/RQRS
1 Ara Drive.
Edwards AFB, CA93524-7013

8. PERFORMING ORGANIZATION REPORT NO.

9. SPONSORING / MONITORING AGENCY NAME(S) AND ADDRESS(ES)
Air Force Research Laboratory (AFMC)
AFRL/RQR
5 Pollux Drive
Edwards AFB CA 93524-7048

10. SPONSOR/MONITOR'S ACRONYM(S)

11. SPONSOR/MONITOR'S REPORT NUMBER(S)
AFRL-RQ-ED-TP-2015-213

12. DISTRIBUTION / AVAILABILITY STATEMENT
Distribution A: Approved for Public Release; Distribution Unlimited.

13. SUPPLEMENTARY NOTES
Technical Paper and Briefing Charts presented at IEPC 2015; Kobe, Japan; 04-10 July 2015. PA#15306.

14. ABSTRACT
Design of efficient Hall-effect thrusters (HETs) is strongly dependent on understanding of electron transport throughout these devices. Among the various mechanisms are proposed to account for enhanced electron transport in the near-field plume of HETs are turbulent fluctuations in the plasma. Since experimental investigations have shown that there is significant energy in azimuthal oscillations of the plasma, it is possible that these azimuthal oscillations in the presence of a radial magnetic field could be the cause of significant axial transport. This paper presents the initial development of a pseudospectral azimuthal-axial hybrid-PIC HET code which is designed to explicitly resolve and filter azimuthal fluctuations in the electrostatic potential. Although development is still far from complete, progress has been made in implementing the electrostatic potential solver. Through significant effort, including the use of both numerical limiters and a smooth fluid neutral description, stable discharges have been demonstrated and interim results are presented.

15. SUBJECT TERMS

16. SECURITY CLASSIFICATION OF:			**17. LIMITATION OF ABSTRACT**	**18. NUMBER OF PAGES**	**19a. NAME OF RESPONSIBLE PERSON**
					Justin Koo
a. REPORT	**b. ABSTRACT**	**c. THIS PAGE**	SAR	26	**19b. TELEPHONE NO** *(include area code)*
Unclassified	**Unclassified**	**Unclassified**			661-275-5908

Standard Form 298 (Rev. 8-98)
Prescribed by ANSI Std. 239.18

Pseudospectral model for hybrid PIC Hall-effect thruster simulation

IEPC-2015-xxx/ISTS-2015-b-xxx

Presented at Joint Conference of 30th International Symposium on Space Technology and Science, 34th International Electric Propulsion Conference and 6th Nano-satellite Symposium
Hyogo-Kobe, Japan
July 4–10, 2015

Justin Koo* and David Bilyeu†
AFRL/RQRS, USA

Robert Martin‡
ERC Incorporated, Huntsville, AL, 35806-3200, USA

Abstract: Design of efficient Hall-effect thrusters (HETs) is strongly dependent on understanding of electron transport throughout these devices. Among the various mechanisms are proposed to account for enhanced electron transport in the near-field plume of HETs are turbulent fluctuations in the plasma. Since experimental investigations have shown that there is significant energy in azimuthal oscillations of the plasma, it is possible that these azimuthal oscillations in the presence of a radial magnetic field could be the cause of significant axial transport. This paper presents the initial development of a pseudospectral azimuthal-axial hybrid-PIC HET code which is designed to explicitly resolve and filter azimuthal fluctuations in the electrostatic potential. Although development is still far from complete, progress has been made in implementing the electrostatic potential solver. Through significant effort, including the use of both numerical limiters and a smooth fluid neutral description, stable discharges have been demonstrated and interim results are presented.

Nomenclature

E = magnitude of electric field
B = magnitude of magnetic field
$\vec{E}$ = electric field
$\vec{B}$ = magnetic field
T_e = electron temperature
p = electron pressure
T_n = neutral temperature
m_n = neutral mass
n_n = neutral density
n_e = electron density
n_i = ion density
k_i = ionization rate
k_B = Boltzmann constant
e = elementary charge
ν = electron momentum exchange collision frequency

*justin.koo@us.af.mil
†david.bilyeu.1@us.af.mil
‡robert.martin.81.ctr@us.af.mil

$\vec{j_e}$ = electron current density
$\vec{j_i}$ = ion current density
μ = scalar electron mobility
$\mu_\perp$ = perpendicular electron mobility
$\mu_\wedge$ = electron mobility perpendicular to both E and B
ϕ = electrostatic potential
m_e = electron mass

I. Introduction

The primary challenge in HET simulation, as with most magnetized plasma devices, is the need to accurately model the transport of electron across magnetic field lines. The presumed mechanisms for this type of transport, known as cross-field electron transport, in HETs are a combination of volumetric electron momentum exchange collisions, electron-wall collisions, and field fluctuations. The first mechanism refers to the idea that when an electron undergoes a collision, it can abruptly shift it's guiding center and thus accomplish net motion against the magnetic field. These collisions can include both electron-ion and electron-neutral collisions, although for most relevant HET plasma conditions, the electron-neutral collisions dominate. The second mechanism, electron-wall collisions, presumes that the interaction between an electron and the device walls is the equivalent to a scattering collision. Finally, the third mechanism refers to the family of field fluctuations (both resolved and unresolved) which, especially in the presence of magnetic fields and fluctuating densities, can lead to net transport effects. The most popular reduced model in HET simulation for unresolved field fluctuation effect is the Bohm diffusion (or Bohm transport) model.

Traditional computational models for HETs fall largely into two categories - full-PIC and hybrid-PIC. While full-PIC is highly desirable in that it actually resolves nonequilibrium behavior for the electron distribution, hybrid-PIC is the far more popular approach as it removes the strict need to resolve high frequency plasma characteristics such as the electron plasma frequency and Debye length. A common feature of most existing hybrid-PIC codes is the treatment of the electrons as a fluid in local thermodynamic equilibrium. This allows for the formulation of an electrostatic solver, based on current conservation, which relies heavily on the details of the relationship between the forcing terms (electric and pressure forces) and the resulting electron current - i.e. the key to the solver is the accuracy of the electron mobility model.

The most popular hybrid-PIC codes in common use, HPHall,[1] relies on this quasi-1D current conservation approach and resolves the radial-axial plane. The formulation explicitly relies on zero derivatives for all quantities in the azimuthal direction. Experimental observations, including Ellison,[2] McDonald[3] and Sekerak,[4] have clearly shown that at readily observable physical and timescales (centimeters and kilohertz), this assumption is not true. Indeed, estimates by MacDonald indicate that a significant fraction of the total discharge energy can be accounted for in azimuthal structures with fairly small wavenumber (corresponding to low order azimuthal modes). For this reason, it seems promising to try to resolve these structures computationally to assess their contribution to overall electron transport in HET operation.

This paper attempts to address the role of resolved field fluctuations in the azimuthal direction as a means for promoting electron transport in a hybrid-HET code. To study this problem, an axial-azimuthal hybrid-PIC HET code is under development, initially with a reduced set of physics. In particular, dynamic ionization is ignored throught the use of imposed electron temperature profiles. Pioneering work in axial-azimuthal simulation has been performed by Coche[5] (full-PIC) and Lam and Fernandez[6] (hybrid-PIC). This work follows the example of Lam and Fernandez but substitutes a spectral description in the azimuthal direction to more naturally resolve oscillations in the plasma.

II. Computational Model

The code developed for this paper is a 2D hybrid-PIC code which resolves an axial-azimuthal plane along the centerline of the HET. As with traditional hybrid-PIC simulations, the ion description (singly charged

xenon only) is with PIC and the electron description is as a fluid with the same density as the ions; however, to avoid the impact of statistical noise in the neutral description on the mobility tensor, the neutrals are modeled with a single temperature (300 K) fluid description rather than the particle description commonly used in other hybrid-PIC HET codes.

A. Electrostatic Potential Solver

Crucially, the electrostatic potential solver is based on the same general current conservation laws as HPHall, but it does not rely on any corrections to the electron mobility with tunable model parameters. The foundation of electrostatic potential solver is current conservation throughout the device which can be written more as:

$$\nabla \cdot (\vec{j_i} + \vec{j_e}) = 0 \tag{1}$$

Assuming that the time derivative of the ion current density is zero, we can replace the divergence of a ion current density with a scalar ionization term to get the overall current conservation equation.

$$\nabla \cdot \vec{j_e} = k_{ioniz} n_e n_n e \tag{2}$$

To get the electron current density as a function of the electrostatic potential (and other driving forces), we begin with a Generalized Ohm's Law description based on the steady state electron momentum equation where $p = n_e k_B T_e$ and $\mu = e/m_e \nu$

$$\vec{j_e} + \mu \vec{j_e} \times \vec{B} = \mu e n_e \vec{E} + \mu \nabla p \tag{3}$$

Expanding this results and performing some arithmentic results in the following expression for the electron current density:

$$\vec{j_e} = \vec{\vec{\mu}} \vec{F} \tag{4}$$

where:

$$F_x = \mu e n_e E_x + \mu \frac{\partial p}{\partial x} = -\mu e n_e \frac{\partial \phi}{\partial x} + \mu \frac{\partial p}{\partial x} \tag{5}$$

$$F_y = \mu e n_e E_y + \mu \frac{\partial p}{\partial y} = -\mu e n_e \frac{\partial \phi}{\partial y} + \mu \frac{\partial p}{\partial y} \tag{6}$$

$$F_z = \mu e n_e E_z + \mu \frac{\partial p}{\partial z} = -\mu e n_e \frac{\partial \phi}{\partial z} + \mu \frac{\partial p}{\partial z} \tag{7}$$

and

$$\vec{\vec{\mu}} = \frac{1}{1 + \mu^2 B_x^2 + \mu^2 B_y^2 + \mu^2 B_z^2} \begin{bmatrix} 1 + \mu^2 B_x^2 & -\mu B_z + \mu^2 B_x B_y & \mu B_y + \mu^2 B_x B_z \\ \mu B_z + \mu^2 B_x B_y & 1 + \mu^2 B_y^2 & -\mu B_x + \mu^2 B_y B_z \\ -\mu B_y + \mu^2 B_x B_z & \mu B_r + \mu^2 B_y B_z & 1 + \mu^2 B_z^2 \end{bmatrix} \tag{8}$$

1. *Simplifications*

To make this model computationally tractable, a number of critical assumptions are now made. First, it is assumed that this is purely an axial-azimuthal model, so there is no conservation equation in the z-direction (Eq. 7). Next, the magnetic field is assumed to everywhere exist only in the z-direction. This changes Eq. 8 from a 3x3 to a 2x2 matrix with the following structure:

$$\vec{\vec{\mu}} = \begin{bmatrix} \frac{1}{1+\mu^2 B^2} & \frac{-\mu B}{1+\mu^2 B^2} \\ \frac{\mu B}{1+\mu^2 B^2} & \frac{1}{1+\mu^2 B^2} \end{bmatrix} = \begin{bmatrix} \mu_{xx} & \mu_{xy} \\ \mu_{yx} & \mu_{yy} \end{bmatrix} = \begin{bmatrix} \mu_\perp & -\mu_\wedge \\ \mu_\wedge & \mu_\perp \end{bmatrix} \tag{9}$$

Subsitution of the above components into Eq. 4 then into Eq. 2 and some rearrangement leads to the following form:

$$\begin{aligned}\frac{\partial}{\partial x}(\mu_\perp \mu e n_e \frac{\partial \phi}{\partial x}) - \frac{\partial}{\partial x}(\mu_\wedge \mu e n_e \frac{\partial \phi}{\partial y}) \\ + \frac{\partial}{\partial y}(\mu_\wedge \mu e n_e \frac{\partial \phi}{\partial x}) + \frac{\partial}{\partial y}(\mu_\perp \mu e n_e \frac{\partial \phi}{\partial y}) = \\ + \frac{\partial}{\partial x}(\mu_\perp \mu \frac{\partial p}{\partial x}) - \frac{\partial}{\partial x}(\mu_\wedge \mu \frac{\partial p}{\partial y}) \\ + \frac{\partial}{\partial y}(\mu_\wedge \mu \frac{\partial p}{\partial x}) + \frac{\partial}{\partial y}(\mu_\perp \mu \frac{\partial p}{\partial y}) + k_i n_e n_n e\end{aligned} \tag{10}$$

Applying the chain rule, moving the cross terms involved with the electrostatic potential to the RHS as a source, and making the subsitutions of $\widetilde{\mu_\perp} = \mu_\perp \mu e n_e$ and $\widetilde{\mu_\wedge} = \mu_\wedge \mu e n_e$, reveals the final form:

$$\begin{aligned}\frac{\partial^2 \phi}{\partial x^2} + \frac{\partial^2 \phi}{\partial y^2} = \\ -\frac{\partial ln(\widetilde{\mu_\perp})}{\partial x}\frac{\partial \phi}{\partial x} + \mu B \frac{\partial ln(\widetilde{\mu_\wedge})}{\partial x}\frac{\partial \phi}{\partial y} - \mu B \frac{\partial ln(\widetilde{\mu_\wedge})}{\partial y}\frac{\partial \phi}{\partial x} - \frac{\partial ln(\widetilde{\mu_\perp})}{\partial y}\frac{\partial \phi}{\partial y} \\ + \frac{1}{\widetilde{\mu_\perp}}\frac{\partial}{\partial x}(\mu_\perp \mu \frac{\partial p}{\partial x}) - \frac{1}{\widetilde{\mu_\perp}}\frac{\partial}{\partial x}(\mu_\wedge \mu \frac{\partial p}{\partial y}) + \frac{1}{\widetilde{\mu_\perp}}\frac{\partial}{\partial y}(\mu_\wedge \mu \frac{\partial p}{\partial x}) + \frac{1}{\widetilde{\mu_\perp}}\frac{\partial}{\partial y}(\mu_\perp \mu \frac{\partial p}{\partial y}) \\ + \frac{k_i n_e n_n e}{\widetilde{\mu_\perp}}\end{aligned} \tag{11}$$

2. Pseudospectral representation

To directly capture the azimuthal modes (which in this case are oriented in the x-direction), the following approximation is used for the electrostatic potential (which also happens to be the same form as a DFT):

$$\phi(x,y) = \frac{1}{N}\sum_{k=0}^{N-1} \hat{\phi}_k(y) e^{\frac{ikx}{L_x}} \tag{12}$$

Where $N * k = L_x$. The boundary conditions are straightforward since $\phi(x,0) = V_{anode}$ and $\phi(x,L_y) = V_{cathode}$ implies that there are only DC components (k=0 mode) of the full Fourier expansion at the anode and cathode boundaries.

$$\hat{\phi}_k(0) = \begin{cases} V_{anode} = 300V & \text{if k} = 0 \\ 0 & \text{if k} \neq 0 \end{cases} \tag{13}$$

and

$$\hat{\phi}_k(L_y) = \begin{cases} V_{cathode} = 0V & \text{if k} = 0 \\ 0 & \text{if k} \neq 0 \end{cases} \tag{14}$$

This formulation solves for the Fourier coefficients of the approximation to ϕ rather than to ϕ itself. During an iteration, the RHS of Eq. 11 is evaluated in physical space then a FFT is applied to the RHS of Eq. 11 in the x-direction at each z location to move the solution to frequency space. This provides N_y sets of N_x Fourier coefficients. The LHS of Eq. 11 is treated as a finite difference scheme (j being the spatial index in the y-direction) for the Fourier coefficients which leads to N sets of tridiagonal matrix inversions of the form:

$$-k^2 \hat{\phi}_{k,j} + \frac{\hat{\phi}_{k,j+1} - 2\hat{\phi}_{k,j} + \hat{\phi}_{k,j-1}}{\Delta y^2} = \widehat{RHS}_k, j \tag{15}$$

3. Recovering electron velocity

Recovering the individual velocity components of the electrons is fairly simple, since:

$$\vec{j_e} = -en_e\vec{u_e} \tag{16}$$

This leads to the formulas:

$$\begin{aligned} u_{e,x} &= \mu_\perp F_x - \mu_\wedge F_y \\ &= -\mu_\perp \mu E_x - \frac{\mu_\perp \mu}{en_e}\frac{\partial p}{\partial x} + \mu_\wedge \mu E_y + \frac{\mu_\wedge \mu}{en_e}\frac{\partial p}{\partial y} \end{aligned} \tag{17}$$

and

$$\begin{aligned} u_{e,y} &= \mu_\wedge F_x + \mu_\perp F_y \\ &= -\mu_\wedge \mu E_x - \frac{\mu_\wedge \mu}{en_e}\frac{\partial p}{\partial x} - \mu_\perp \mu E_y - \frac{\mu_\perp \mu}{en_e}\frac{\partial p}{\partial y} \end{aligned} \tag{18}$$

B. Neutral Flow Solver

Neutral advection is perfromed using a high-order semi-Lagrangian advection scheme developed by Qiu.[7] In addition to the semi-Lagrangian advection, a simple Knudsen diffusion model, shown in Eq. 19, is applied to the neutral population. In practice, given the timescale of the simulation, this is a very minor correction on the neutral density and has minimal impact on the evolution of the solution.

$$\frac{\partial n_{xe}}{\partial t} = -D_{Kn}\nabla^2 n_{Xe} \approx -v_{th}L_{channel}\nabla^2 n_{Xe} \tag{19}$$

III. Implementation

The basic geometry of the simulation is 10 cm in the θ-direction (representing the azimuthal channel dimension) and 4.5 cm in the z-direction (representing the axial channel dimension). The underlying computational grid is divided into 1 mm segments in the x- and y-directions and there is a single cell of height 2 cm in the z-direction. The prescribed magnetic field does not account for inductive effects and remains constant through the simulation. Further, there is no evolution equation for the electron temperature but it maintains the shape prescribed at the start of the simulation. Given this lack of a self-consistent electron energy solver, it is only necessary to resolve the ion timescale motion so a timestep of 50 ns was used throught the simulation. The initial conditions chosen for each are shown in Fig. 1. The model used to evaluate the ionization rate are from Appendix E of Goebel.[8]

1. Particle boundary conditions

A constant boundary condition of 25 mg/s and $n = 3e19/m^3$ of Xe at 300K with an inflow velocity of 1911 m/s is used to represent neutral injection at the anode corresponding to the 5 mg/s case described by Coche[5] for a $2cm$ wide segment in the θ-direction. Because that work provides neither inflow velocity or equivalent channel thickness for the 2D model, it is unclear whether this flow-rate is 5x that of their work with the 5mg/s number implied for the full annulus rather than the segment. To avoid regions of zero electron density, a similar boundary condition is used to inject a small amount of Xe^+ into the solution at anode - this seed population is sampled form a reservoir with a density of 1E18 $1/m^3$, a temperature of 11605 K and an inflow drift velocity of 1911 m/s. Periodic particle boundary conditions are used in the θ-direction. In the radial direction, specular reflection for the neutrals and recombination (to a surface temperature of 300 K) of the ions were used. A novel particle merge/splitting algorithm was also investigated to constrain the total number of macroparticles in the simulation - details of this work are provided in a companion paper.[9]

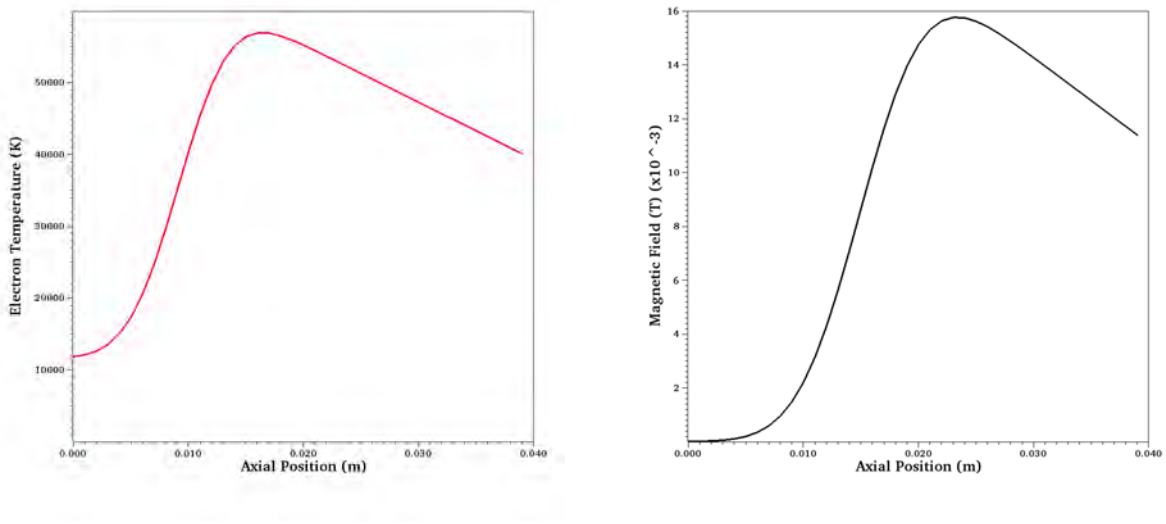

Figure 1. Imposed electron temperature and magnetic field

2. Solution methodology

To account for the fact that the electrostatic potential in Eq. 11 appears on both the left-hand side (as the solution variable) and right-hand side (as a source term) of the equation, a fixed point iterative solve is used to converge the solution at each iteration. For the terms in the right side of the equation, simple finite-difference evualutations were used. In the future, θ-derrivatives should also be calculated in frequency space to improve accuracy, but with the square spatial cells used in this work, improved accuracy in only a single direction would have a minor impact on the overall error while dramatically increasing the complexity. Though spectral accuracy is lost, the pseudospectral solve allows for single-step solution across space for a given right hand side enabling rapid convergence of the fixed-point iteration.

Though this iteration as described was successful for non-ionizing cases, the iteration would diverge when the $\partial ln(\widetilde{\mu_\perp})/\partial y$ term exceeded a magnitude of approximately 1.0 as is the case in regions of steep ionization gradient. To stabilize the solver, an ad-hoc arctangent limiter shown in Equation was applied to the perpendicular log mobility gradient terms multiplying the electric field in the RHS. Once limited, only a few iterations were typically needed to bring the L_2 residual down to an acceptable tolerance as shown in the results section. The impact on the solution of the limiter will be assessed in future work, but presumeably if the physical gradients were sufficiently resolved, the log of the gradient could be made arbitrarily small. Unfortunately, the particle noise is also inversely related to the cell size which can also cause the term to become large. The impact of the limiter on the solution is left to future work.

$$\left.\frac{\partial ln(\widetilde{\mu_\perp})}{\partial y}\right|_{limiter} \approx \frac{1}{\pi \Delta y}\texttt{atan}\left(\frac{\pi}{2} ln(\widetilde{\mu_\perp}(y+\Delta y)/\widetilde{\mu_\perp}(y-\Delta y))\right) \tag{20}$$

The code is single-threaded and requires only standard desktop computing resources, but uses the FFTW compatible inferface to the cuda accelreated cuFFT library[10] for the spectral field solve. In the spectral solve, both boundary conditions and the right hand side source terms are de-aliased using the 2/3rd dealiasing rule.[11]

IV. Results

Considerable effort was expended to demonstrate that this code could be run stably for even a short period of time. Once the mobility gradient was limited, the solution remained stable over a wide range of parameters. Below shows the fixed-point iteration cycle output for the 300^{th} iteration corresponding $t = 15\mu s$, as a representative example using the criteria $\left\|(\Phi^n - \Phi^{n-1}\right\|_{L^2}$ <1.0e-02 shown in Table 1.

Fig. 2 shows the time evolution of the solution. After an initial startup transient due to inconsistency be-

```
Iteration 300:   Time=1.500005e-05 dt=5.000000e-08 [Wall Clock:3770.176944]
                 NORM: 3.953806e-01
                 NORM: 4.586822e-01
                 NORM: 2.932743e-01
                 NORM: 5.065295e-02
                 NORM: 1.004307e-01
                 NORM: 5.369610e-02
                 NORM: 3.419605e-02
                 NORM: 3.912887e-02
                 NORM: 6.203489e-03
Iteration 301:   Time=1.505005e-05 dt=5.000000e-08 [Wall Clock:3782.982616]
```

Table 1. Pseudo-spectral fixed-point iteration for electrostatic potential.

tween the initial neutral density and steady solution, the discharge becomes quite stable in time. Relatively little variation in the solution after approximately $t = 15\mu s$ was observed in runs as far out as $200\mu s$. The lack of an observed breathing mode is attributed to the constant imposed temperature profile used in place of solving the electron energy equation, but confirmation of this observation is left to future work studying the full coupled system.

As the solution transient clear the domain after approximately $15\mu s$, Fig. 3 shows Ions and neutral densities in the $\theta - z$ plane where the anode is represented by the bottom surface and cathode by the top. The ionization front depletes the neutral population, but never attains the density of the original distribution because they are rapidly accelerated out of the domain by the electric field. The results show little structure in the θ-direction which probably aids in the progression towards completely stable plasma discharge. The coupling of field to ion density alone appears to not break the symmetry of the problem. Once the energy equation is included in the model, it will be interesting to see if azimuthal structure will be recovered due to the rapid ionization quenching the electron temperature locally.

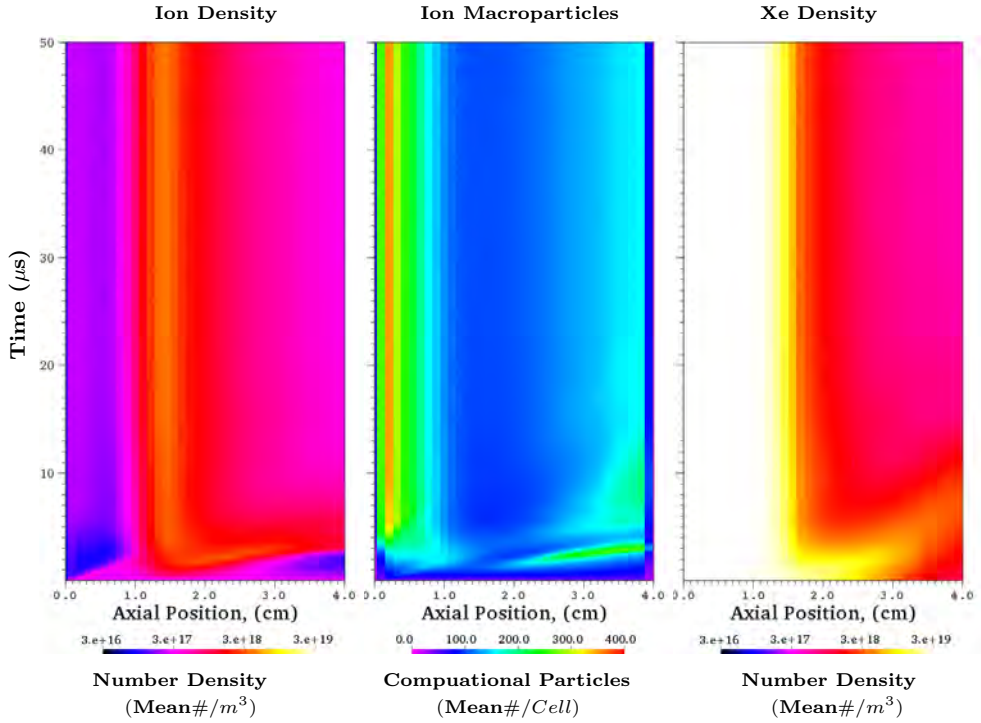

Figure 2. PIC ion densities, macroparticle counts, and neutral Xe densities. Data is averaged over θ-direction and plotted over time.

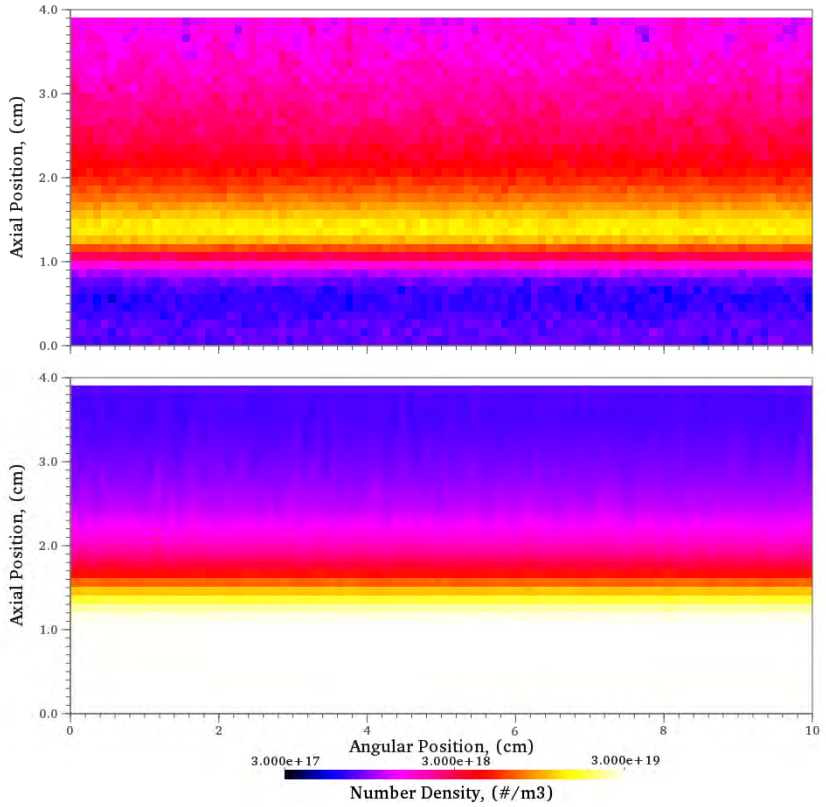

Figure 3. Ion (top) and neutral Xe (bottom) densities at $t = 15\mu s$. Mean flow is from bottom (anode) to top (cathode).

V. Conclusions and Future Work

These result represent a preliminary investigation into a pseudospectral axial-azimuthal hybrid-PIC methodology for a Generalized Ohm's law solver. Initial development required reliance on numerical artifice (artificial limiters on some source terms for the electrostatic potential solver) to achieve a stable solution. Not surprisingly, without a coupled energy (electron temperature) equation, this effort was unable to produce characteristic breathing mode oscillations.

Significant future work is anticipated for this effort. In addition to the clear need to incorporate a coupled electron energy equation, the impact the ad-hoc limiter must also be investigated. It is unclear whether this limiter will continue to be necessary or whether a similar effect can be accomplished with a more physically motivated wall-loss terms in the energy equation. Nevertheless, this work represents an important initial step towards a new research tool to better understand the plasma processes in HET discharges.

References

[1]Fife, J. M., *Hybrid-PIC Modeling and Electrostatic Probe Survey of Hall Thrusters*, Ph.D thesis, Massachusetts Institute of Technology, Department of Aeronautics and Astronautics, 1998.

[2]Ellison, C. L., Raitses, Y., and Fisch, N. J., "Cross-field electron transport induced by a rotating spoke in a cylindrical Hall thruster," *Physics of Plasmas*, Vol. 19, No. 1, 2012, pp. 013503–1–013503–7.

[3]McDonald, M. S., *Electron transport in Hall thrusters*, Ph.D thesis, University of Michigan, Department of Applied Physics, 2012.

[4]Sekerak, M. J., Longmier, B. W., Gallimore, A. D., Brown, D. L., Hofer, R. R., and Polk, J. E., "Azimuthal Spoke Propagation in Hall Effect Thrusters," *IEEE Transactions on Plasma Science*, Vol. 43, No. 1, 2015, pp. 72–85.

[5]Coche, P. and Garrigues, L., "A two-dimensional (azimuthal-axial) particle-in-cell model of a Hall thruster," *Physics of Plasmas*, Vol. 21, 2014, pp. 023503–1–023503–10.

[6]Lam, C. M., Fernandez, E., and Cappelli, M. A., "A 2-D Hybrid Hall Thruster Simulation That Resolves the ExB Electron Drift Direction," *IEEE Transactions on Plasma Science*, Vol. 43, No. 1, 2015, pp. 86–94.

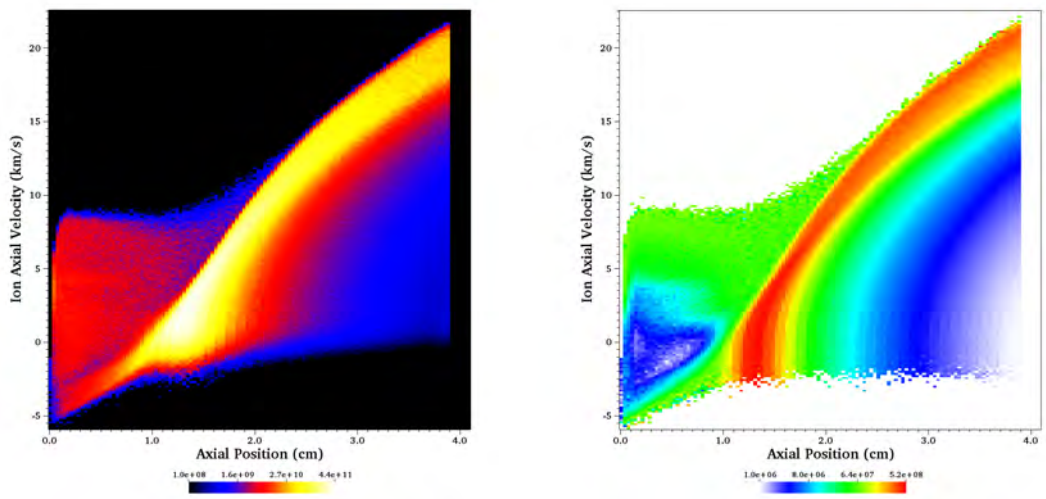

Figure 4. Axial velocity distribution (VDF). Left shows ion VDF bin density and right shows bin averaged macroparticle physical to computatational weight ratio.

[7]J.-M. Qiu, A. Christlieb, "A conservative high order semi-Lagrangian WENO method for the Vlasov equation," *J. Comp. Phys.*, Vol. 229, 2010, pp. 1130–1149.

[8]Goebel, D. M. and Katz, I., *Fundamentals of Electric Propulsion: Ion and Hall Thrusters*, John Wiley & Sons, Inc., 2008.

[9]Martin, R., J.W., K., Bilyeu, D., and Tran, J., "Dynamic Particle Weight Remapping in Hybrid PIC Hall-effect Thruster Simulation," *34^{th} Int. Electric Propulsion Conf. (IEPC)*, Kobe, Japan, July 2015, pp. IEPC–2015–XXX.

[10]NVIDIA Corporation, *cuFFT Library User's Guide*, 2015, Version 7.0.

[11]Bewley, T., *Numerical Renaissance: simulation, optimization, & control*, Renaissance Press, 2014.

Pseudospectral model for hybrid PIC Hall-effect thruster simulation

06-10 Jul 2015

Justin Koo and Robert Martin

EP Modeling and Simulation group

AFRL/RQRS

Outline

- Background on azimuthal oscillations
- Existing azimuthal-axial codes
- Motivation for new model
- Model development
  - Formulation of governing equations
  - Implementation details
- Initial results
- Summary and future work

Motivation

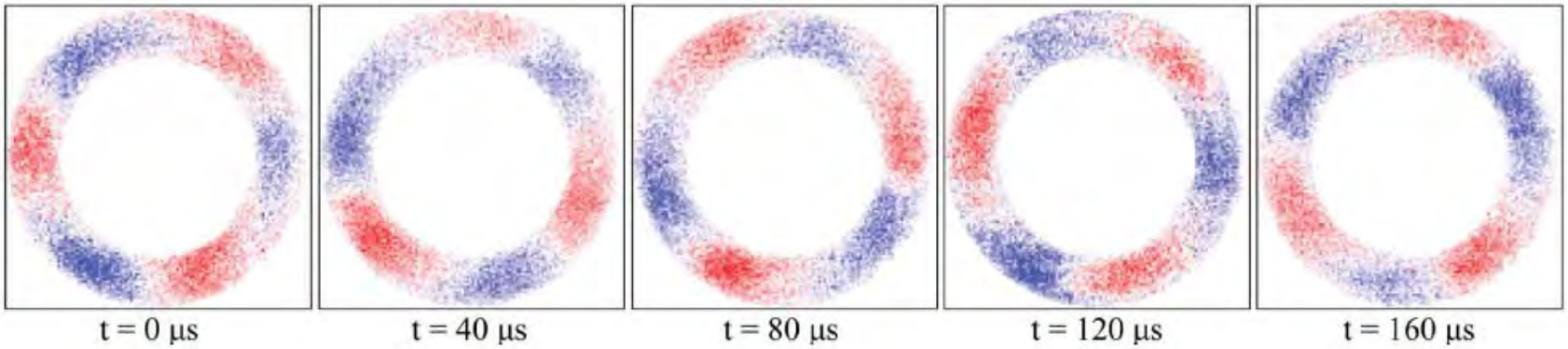

Fig. 2. False-color ac-coupled video of a 600-V 10-A operating condition at 27 000 fps shows a coherent threefold spoke structure rotating in the counterclockwise direction. The frequency of spoke passage by a given point on the channel is approximately 3 kHz, but each spoke's individual rotational frequency is only one-third this value, or 1 kHz, corresponding to a velocity of about 500 m/s.

McDonald, M.S.; Gallimore, A.D., "Rotating Spoke Instabilities in Hall Thrusters," *Plasma Science, IEEE Transactions on* , vol.39, no.11, pp.2952,2953, Nov. 2011

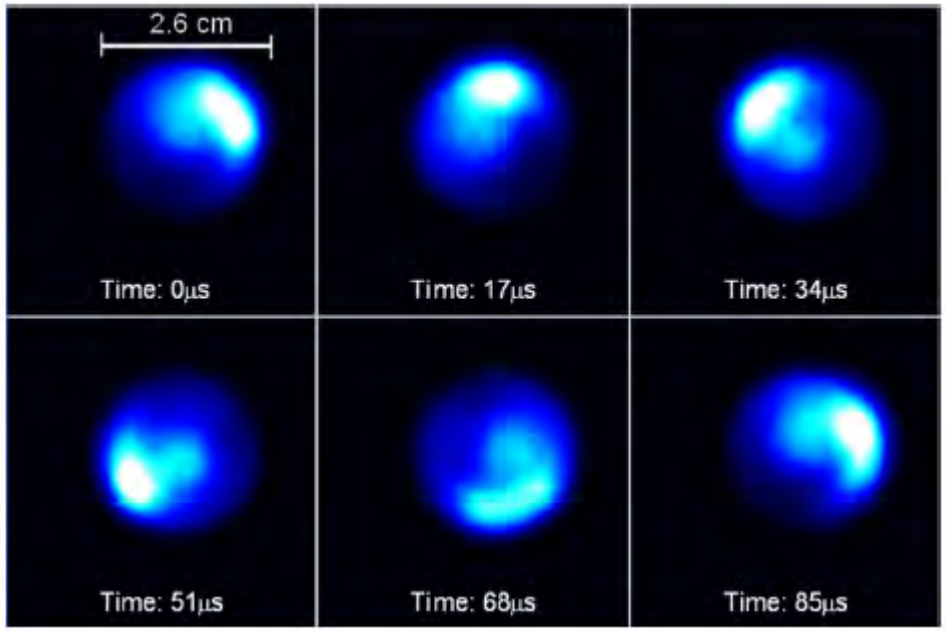

Cross-field electron transport induced by a rotating spoke in a cylindrical Hall thruster, Ellison, C. L. and Raitses, Y. and Fisch, N. J., Physics of Plasmas (1994-present), 19, 013503 (2012)

Recent azimuthal-axial codes

Full PIC

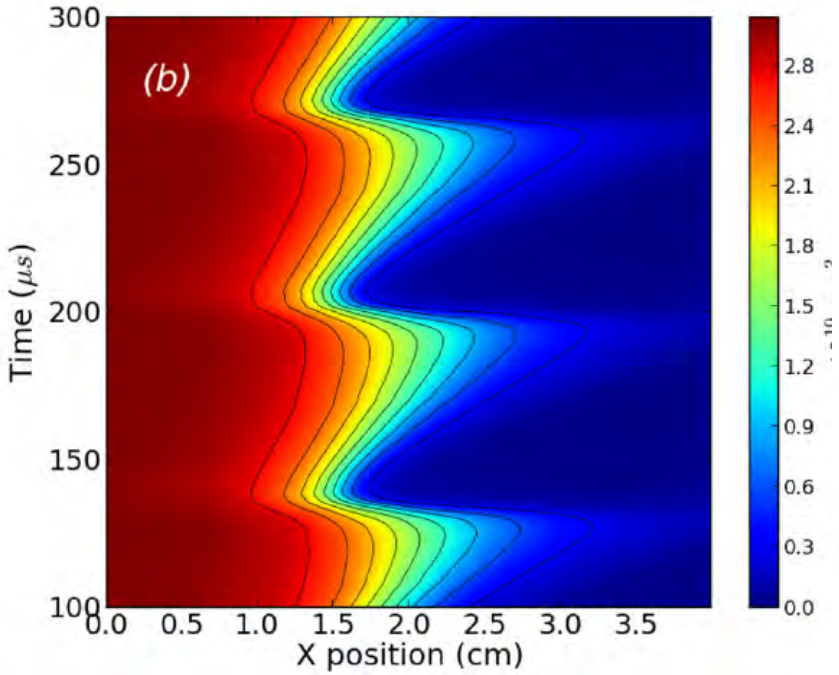

A two-dimensional (azimuthal-axial) particle-in-cell model of a Hall thruster, Coche, P. and Garrigues, L., Physics of Plasmas (1994-present), 21, 023503 (2014)

Hybrid-PIC

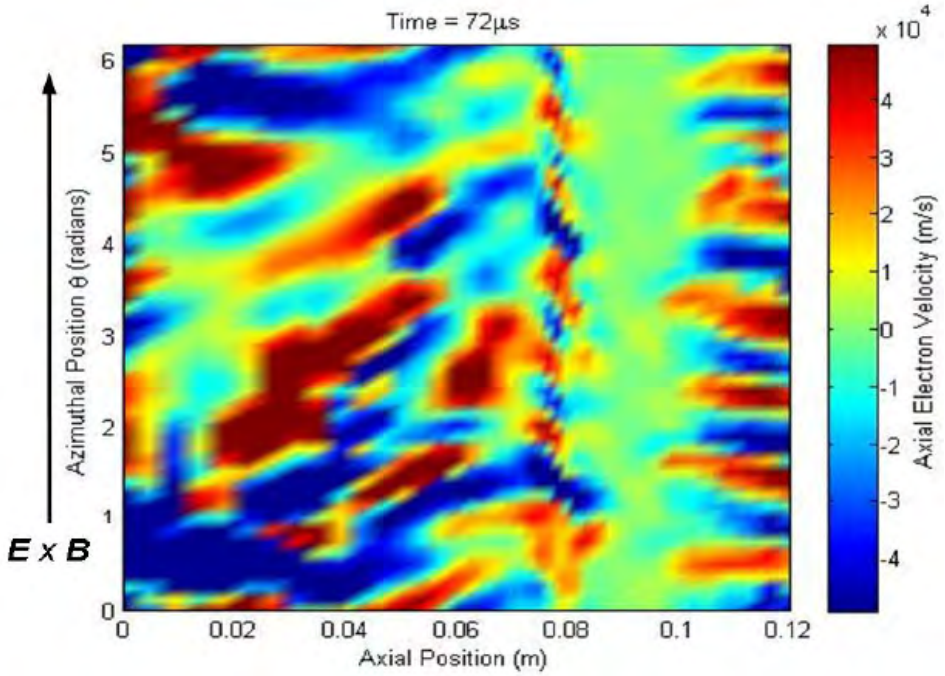

A 2D Hybrid Hall Thruster Simulation That Resolves the ExB Electron Drift Direction, Lam, C., Fernandez, E. and Cappelli, M., IEEE Transactions of Plasma Science, Vol 43 (1), 86-94 (2015)

Motivation for new model

- Based on experimental observations, it appears that we need only resolve the first few (m<10) azimuthal modes to capture spoke instability – seems a natural fit for a spectral description
- PIC simulations are inherently noisy – this makes it even more difficult to deal with the stiffness of the mobility tensor; pseudospectral description would have the added benefit of smoothing the distribution
- Given time constraints, first attempt at implementing pseudospectral model would be a partial attempt:
  - Imposed magnetic field and electron temperature profile (actually introduced additional difficulties)

Overall concept

- Azimuthal-axial (x-y) computational domain
  - Actually an x-y-z code where z is one large cell (2 cm) across
- Hybrid-PIC code
  - Electron are quasineutral fluid characterized by an imposed temperature profile
  - Ions are macroparticles (PIC)
  - Neutrals are a fluid (semi-Lagrangian advection and simple Knudsen diffusion model)
  - Electrostatic potential is constructed of Fourier basis functions in azimuthal direction

Formulation of electron mobility

From Generalized Ohm's law:

$$\vec{j_e} + \mu \vec{j_e} \times \vec{B} = \mu e n_e \vec{E} + \mu \nabla p$$

Retrieve full Cartesian form of electron mobility

$$\vec{j_e} = \vec{\vec{\mu}} \vec{F}$$

$$F_x = \mu e n_e E_x + \mu \frac{\partial p}{\partial x} = -\mu e n_e \frac{\partial \phi}{\partial x} + \mu \frac{\partial p}{\partial x}$$

$$F_y = \mu e n_e E_y + \mu \frac{\partial p}{\partial y} = -\mu e n_e \frac{\partial \phi}{\partial y} + \mu \frac{\partial p}{\partial y}$$

$$F_z = \mu e n_e E_z + \mu \frac{\partial p}{\partial z} = -\mu e n_e \frac{\partial \phi}{\partial z} + \mu \frac{\partial p}{\partial z}$$

$$\vec{\vec{\mu}} = \frac{1}{1 + \mu^2 B_x^2 + \mu^2 B_y^2 + \mu^2 B_z^2} \begin{bmatrix} 1 + \mu^2 B_x^2 & -\mu B_z + \mu^2 B_x B_y & \mu B_y + \mu^2 B_x B_z \\ \mu B_z + \mu^2 B_x B_y & 1 + \mu^2 B_y^2 & -\mu B_x + \mu^2 B_y B_z \\ -\mu B_y + \mu^2 B_x B_z & \mu B_r + \mu^2 B_y B_z & 1 + \mu^2 B_z^2 \end{bmatrix}$$

2D electron mobility (x-y)

Assuming an azimuthal axial model where the x-direction represents the azimuthal direction and the y-direction represents the axial direction and assuming that the B field is all in the z-direction

$$\vec{\vec{\mu}} = \begin{bmatrix} \mu_{xx} & \mu_{xy} \\ \mu_{yx} & \mu_{yy} \end{bmatrix} = \begin{bmatrix} \mu_{\perp} & -\mu_{\wedge} \\ \mu_{\wedge} & \mu_{\perp} \end{bmatrix}$$

$$\mu_{\perp} = \frac{1}{1 + (\mu B)^2}$$

$$\mu_{\wedge} = \frac{\mu B}{1 + (\mu B)^2}$$

Starting from current conservation, after much manipulation this is the formulation for the potential solver:

$$\frac{\partial^2 \phi}{\partial x^2} + \frac{\partial^2 \phi}{\partial y^2} = -\frac{\partial ln(\widetilde{\mu_{\perp}})}{\partial x}\frac{\partial \phi}{\partial x} + \mu B \frac{\partial ln(\widetilde{\mu_{\wedge}})}{\partial x}\frac{\partial \phi}{\partial y} - \mu B \frac{\partial ln(\widetilde{\mu_{\wedge}})}{\partial y}\frac{\partial \phi}{\partial x} - \frac{\partial ln(\widetilde{\mu_{\perp}})}{\partial y}\frac{\partial \phi}{\partial y} + \frac{1}{\widetilde{\mu_{\perp}}}\frac{\partial}{\partial x}(\mu_{\perp}\mu\frac{\partial p}{\partial x}) - \frac{1}{\widetilde{\mu_{\perp}}}\frac{\partial}{\partial x}(\mu_{\wedge}\mu\frac{\partial p}{\partial y}) + \frac{1}{\widetilde{\mu_{\perp}}}\frac{\partial}{\partial y}(\mu_{\wedge}\mu\frac{\partial p}{\partial x}) + \frac{1}{\widetilde{\mu_{\perp}}}\frac{\partial}{\partial y}(\mu_{\perp}\mu\frac{\partial p}{\partial y}) + \frac{k_i n_e n_n e}{\widetilde{\mu_{\perp}}}$$

$$\boxed{\widetilde{\mu_{\perp}} = \mu_{\perp}\mu e n_e \text{ and } \widetilde{\mu_{\wedge}} = \mu_{\wedge}\mu e n_e}$$

Pseudospectral representation

Fourier mode basis functions for potential in x-direction:

$$\phi(x,y) = \frac{1}{N}\sum_{k=0}^{N-1} \hat{\phi}_k(y) e^{\frac{ikx}{L_x}} \qquad N * k = L_x$$

K=0 boundary conditions only on y-ends of solution:

$$\hat{\phi}_k(0) = \begin{cases} V_{anode} = 300V & \text{if k} = 0 \\ 0 & \text{if k} \neq 0 \end{cases} \qquad \hat{\phi}_k(L_y) = \begin{cases} V_{cathode} = 0V & \text{if k} = 0 \\ 0 & \text{if k} \neq 0 \end{cases}$$

Potential solver in y-direction is simply finite-difference of Fourier coefficients:

$$-k^2\hat{\phi}_{k,j} + \frac{\hat{\phi}_{k,j+1} - 2\hat{\phi}_{k,j} + \hat{\phi}_{k,j-1}}{\Delta y^2} = \widehat{RHS}_{k,j}$$

RHS contains ϕ so point nonlinear iteration used to converge solution

Initial/Boundary Conditions

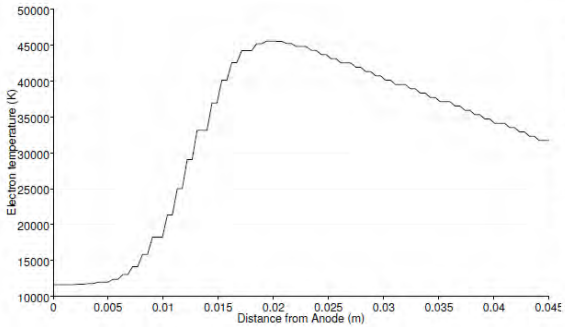

Electron Temperature (Max 4eV)

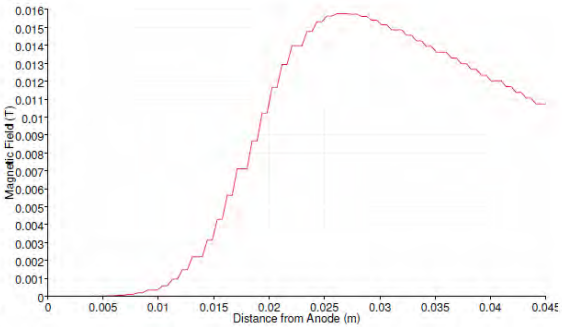

Magnetic Field (Max 160 G)

In z-direction, ion recombination to form 300K Xe

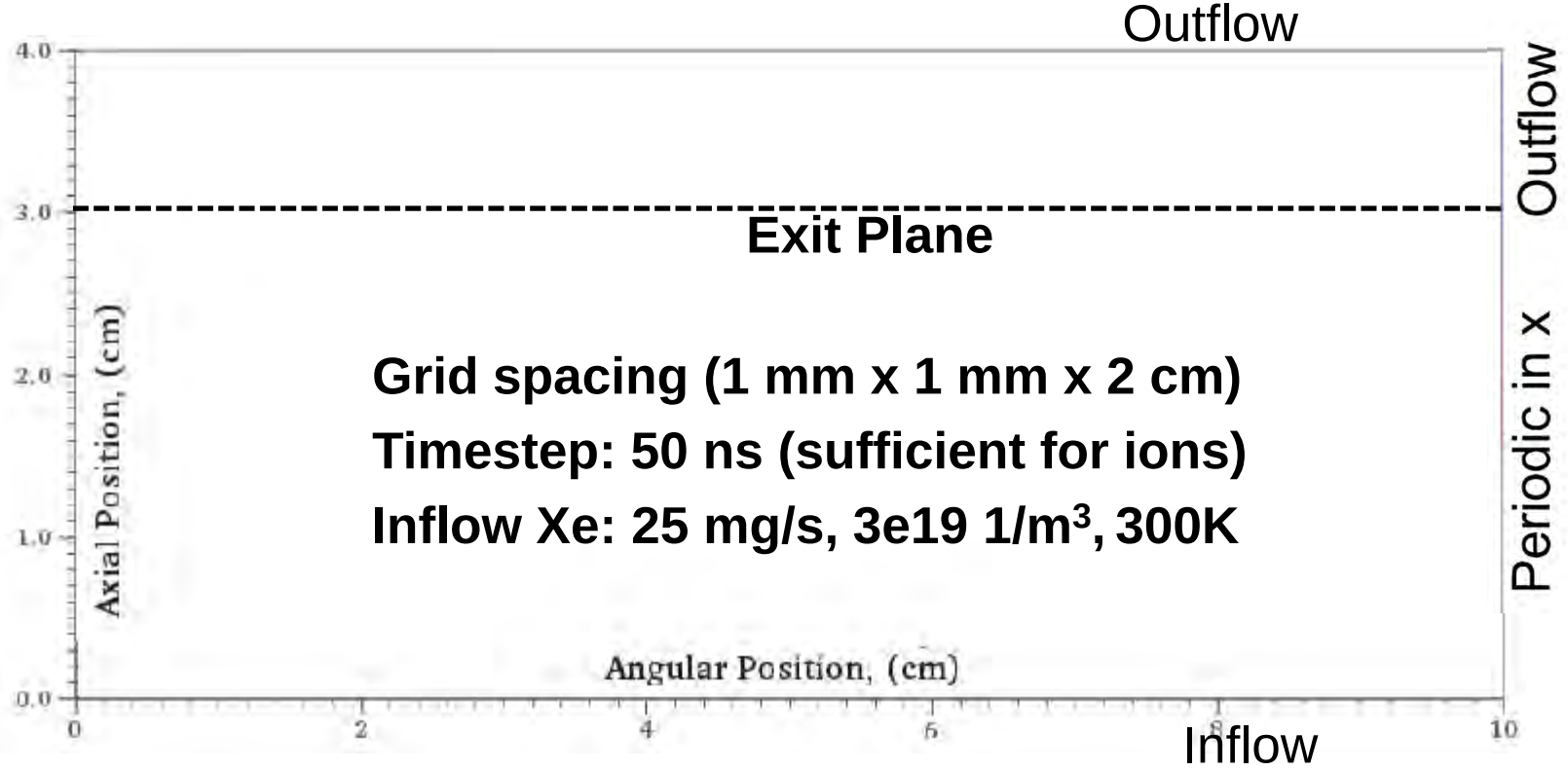

Compromises to stability

Generating stable solution was much harder than anticipated – numerous numerical tricks were employed to achieve stability

- To avoid regions with no Xe+, Xe+ was injected into the simulation from the anode from a reservoir with density 1E18 $1/m^3$, 11605 K and drift velocity of 1911 m/s
- Neutrals were initially PIC but switched to fluid description
- Limiter used to restrain unruly term on RHS

$$\left.\frac{\partial ln(\widetilde{\mu_\perp})}{\partial y}\right|_{limiter} \approx \frac{1}{\pi \Delta y}\mathtt{atan}\left(\frac{\pi}{2} ln(\widetilde{\mu_\perp}(y+\Delta y)/\widetilde{\mu_\perp}(y-\Delta y))\right)$$

- Upper 1/3 of Fourier coefficients are filtered to prevent aliasing

Neutral density
t = 15 microseconds

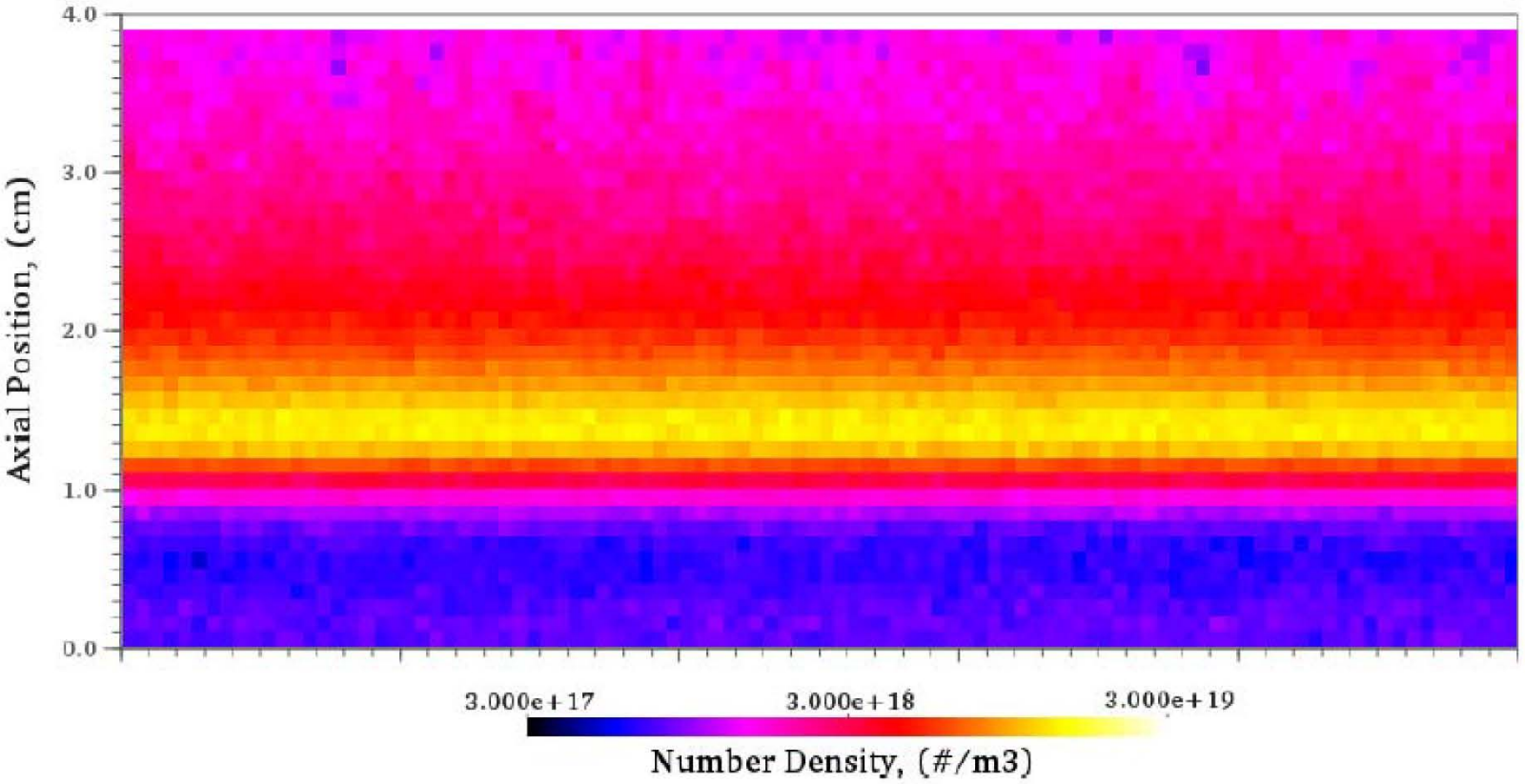

Ion density
t = 15 microseconds

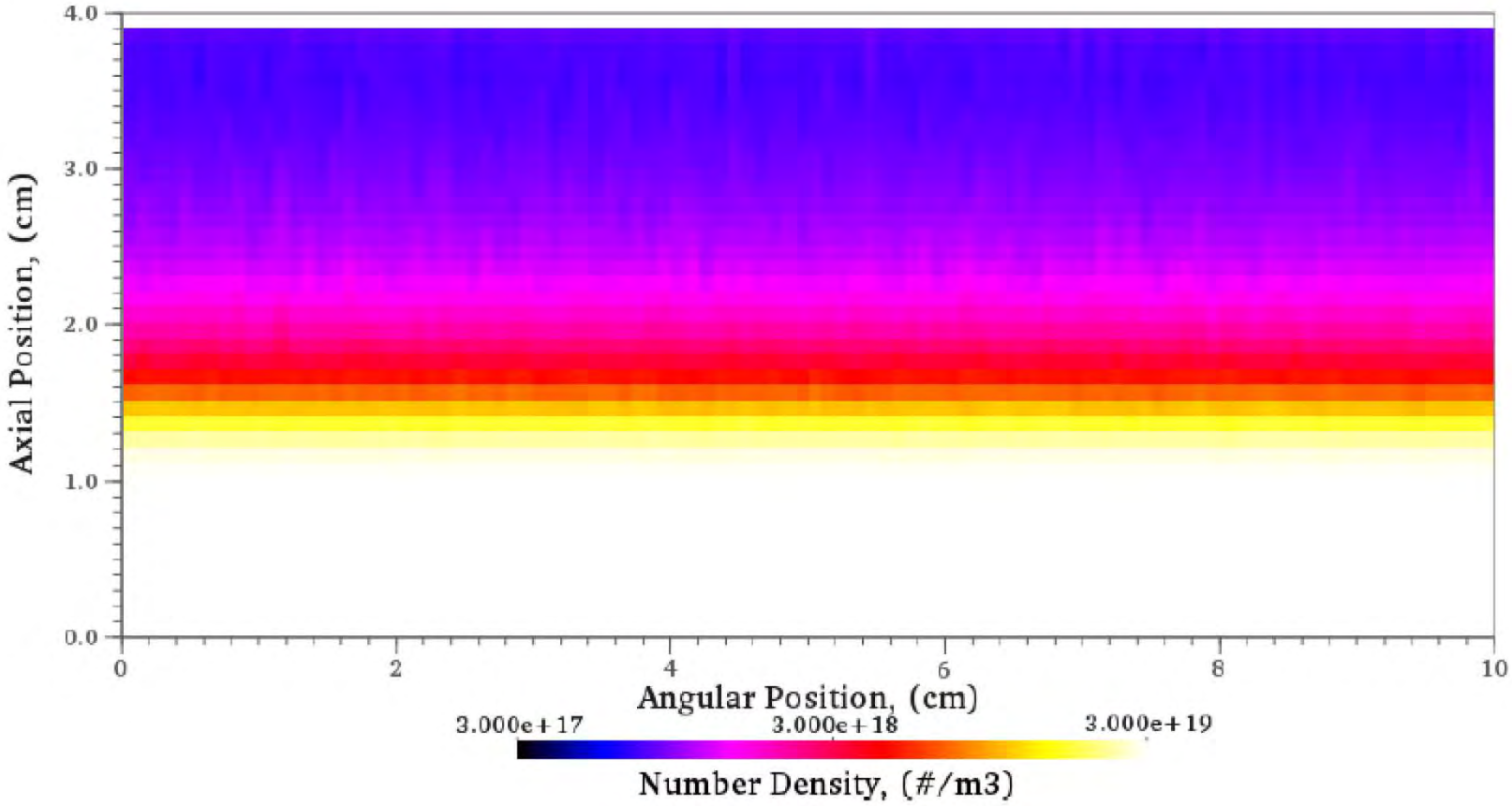

Azimuthal-average profiles

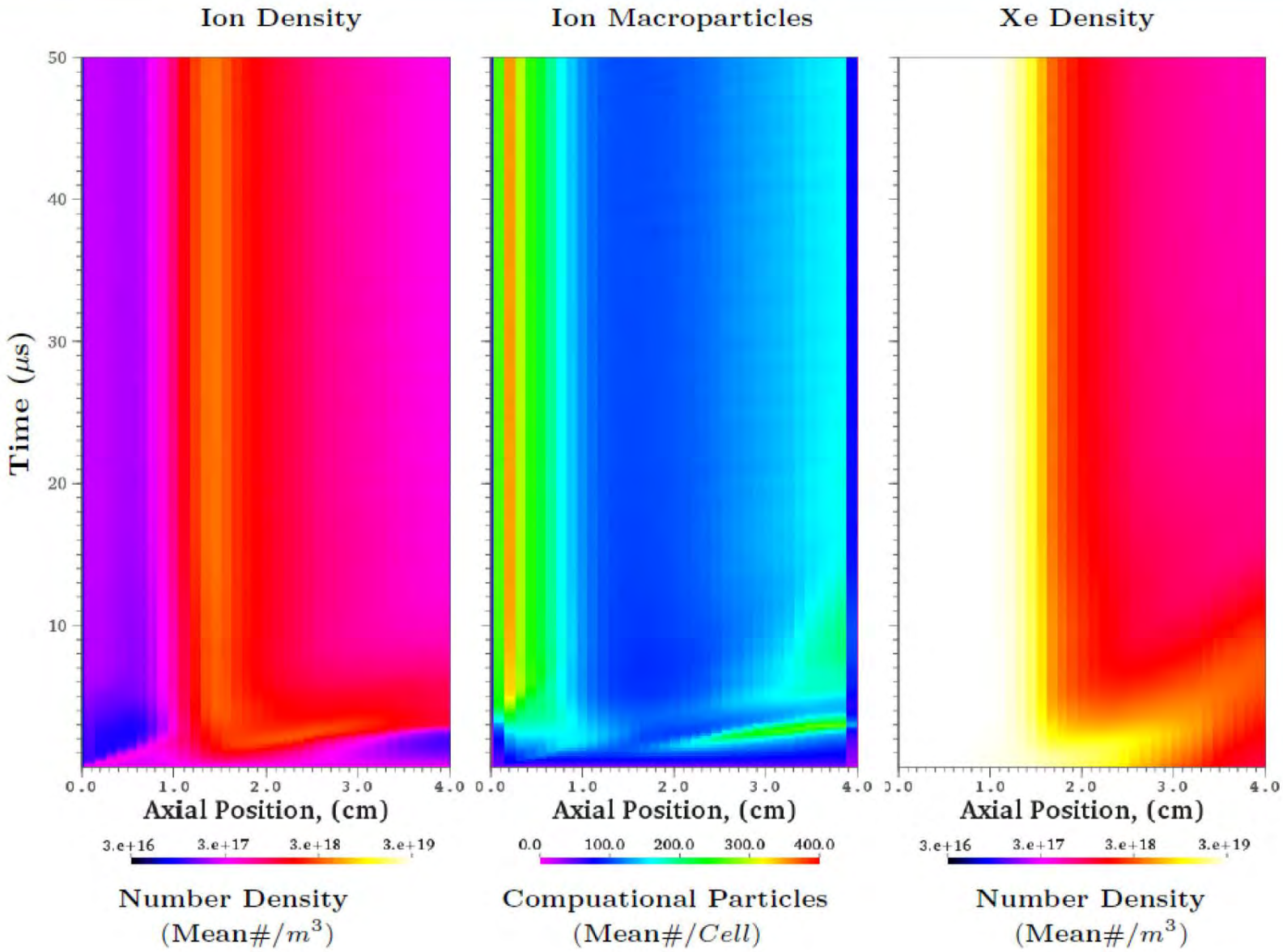

Axial Ion VDFs

Density

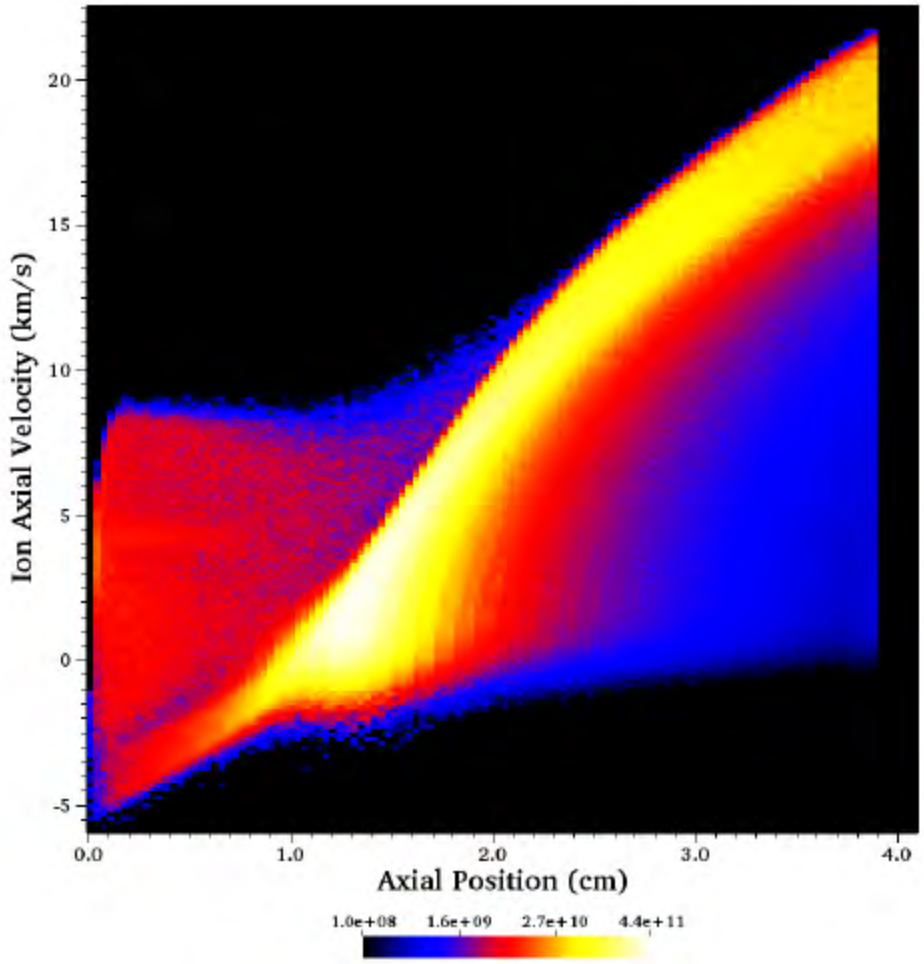

Average macroparticle weight

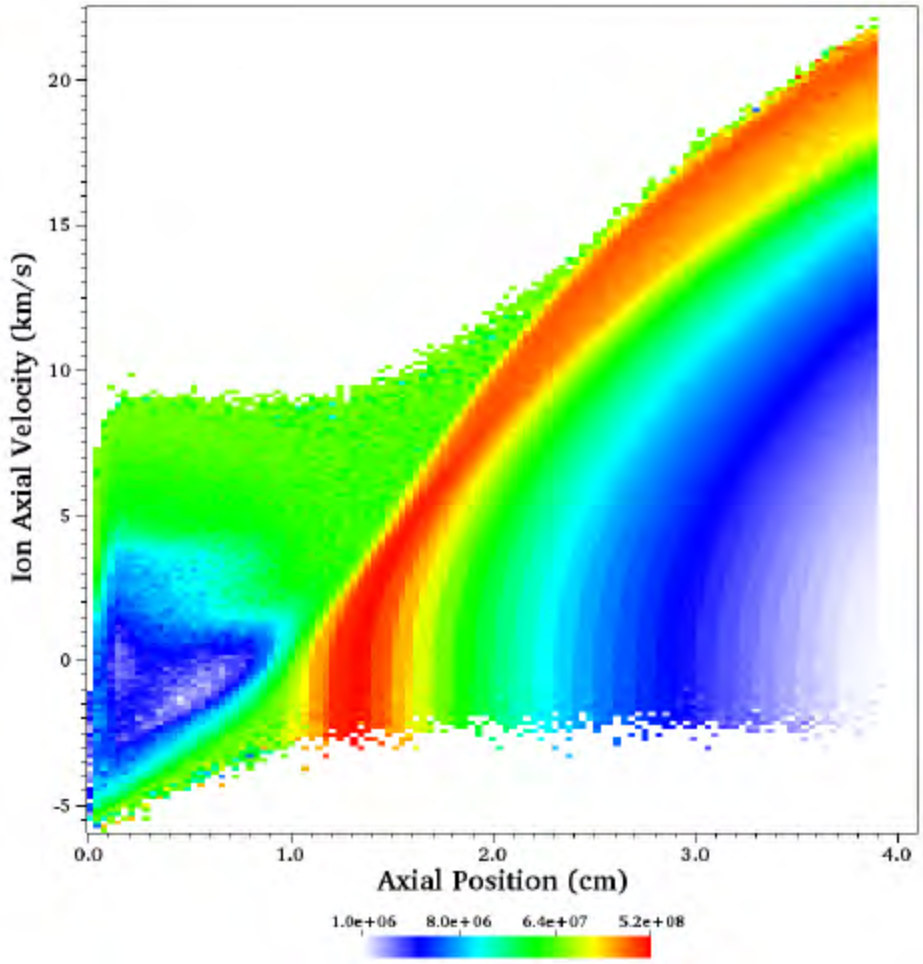

Summary and Future Work

- Initial efforts to construct a hybrid-PIC azimuthal-axial HET code with a pseudospectral potential representation have met mixed success
  - Achieved stable discharge
  - Several undesirable fixes to stabilize discharge
- Significant future work is planned
  - Time dependent electron temperature equation
  - Pseudospectral representation for terms evaluated on the RHS of the potential equation / removal of ad-hoc limiters for term on RHS